Research Square

Preprints are preliminary reports that have not undergone peer review.
They should not be considered conclusive, used to inform clinical practice,
or referenced by the media as validated information.

Metrology-Driven Optical NDE for Screening ICT Probe-Induced Indentations on PCB Pads

Rafael Silva
Digital transformation colab
António Silva
Digital transformation colab
Luís Cura
Digital transformation colab
Cátia Loureiro
Digital transformation colab
António Araújo
Bosch Car Multimedia BrgP
Paulo Pedrosa
Digital transformation colab
Duarte Fernandes
duarte.fernandes@dtx-colab.pt

Digital transformation colab

Research Article

Keywords: in-circuit test, computer vision, nondestructive evaluation, surface integrity, quantitative inspection, defect characterization

Posted Date: March 22nd, 2026

DOI: https://doi.org/10.21203/rs.3.rs-8502691/v1

License: This work is licensed under a Creative Commons Attribution 4.0 International License. Read Full License

Additional Declarations: No competing interests reported.

Abstract

In-circuit testing (ICT) is widely used for electronics quality control, yet spring-loaded probes may introduce micro-indentations on test pads that can compromise surface integrity and, in critical cases, expose copper and lead to latent failures. This paper presents a quantitative, non-contact optical nondestructive evaluation (NDE) method to screen ICT-induced pad damage by combining calibrated microscopy with metrology-driven feature extraction and interpretable classification. High-resolution images are acquired using an optical microscope with an effective resolution of ≈ 1.67 μm/pixel, and a dedicated experimental setup is used to generate a dataset of over 2000 images spanning multiple pad coatings, probe types, and applied forces. The proposed vision-based measurement pipeline is validated against reference measurements, achieving an absolute error of 1.5 μm for indentation height (2.1% MRE) with a − 0.3 μm bias, and showing < 2% dimensional variation, indicating good repeatability. From the measured indentation geometry and appearance, a set of physically meaningful features is computed and used to train an interpretable decision-tree model to classify indentations as acceptable (OK) or critical (NOK). Across the evaluated conditions, the method reaches 98–100% classification accuracy while remaining lightweight and traceable, supporting practical deployment as an optical NDE quality gate for test-induced surface damage after ICT.

I. INTRODUCTION

In-Circuit Testing (ICT) is a quality control method in the electronics manufacturing industry, ensuring that printed circuit boards (PCBs) function correctly prior to final assembly. The process relies on a bed-of-nails fixture, which is an array of spring-loaded test probes (or needles) arranged in a pattern that corresponds to the test pads on the PCB (namely component leads, test pads, through-holes, etc.).

This work was supported under the base funding project of the DTx CoLAB, under the Missão Interface of the Recovery and Resilience Plan (PRR), integrated in the notice 01/C05-i02/2022, which aims to deepen and consolidate the network of interface institutions between the academic, scientific and technological system and the Portuguese business fabric.

Rafael Silva, António Silva, Luís Cura, Cátia Loureiro, Paulo Pedrosa and Duarte Fernandes are with Digital Transformation CoLab, Guimarães, Portugal (e-mail: rafael.silva@dtx-colab.pt; antonio.silva@dtx-colab.pt; luis.cura@dtx-colab.pt;catia.loureiro@dtx-colab.pt;paulo.pedrosa@dtx-colab.pt; duarte.fernandes@dtx-colab.pt).

António Araújo is with Bosch Car Multimedia Portugal S.A., Braga, Portugal (e-mail:antonio.araujo3@pt.bosch.com).

The needles ensure a reliable electrical connection between the fixture and the PCB, enabling the measurement of various electrical parameters, such as voltage, current, resistance, and continuity. While this technique offers several advantages (e.g., fast testing speed, high repeatability) [1], needles may fail after extended periods of usage. The failure of test needles can cause unintended damage to PCB test pads, such as excessive wear, pad lifting and microcracks in solder joints, which may result in long-term reliability issues in electronic assemblies. The consequences of needle failure extend beyond immediate test inaccuracies considering that physical damage to the PCB can lead to latent defects that are difficult to detect during quality control, ultimately resulting in field failures.

A. Problem Description

Depending on the type of product, the bed-of-needles used can comprise hundreds of spring-loaded probes and reach thousands of inspection cycles without requiring maintenance. During inspection, each needle exerts a force of up to 4 N over the PCB surface, which is sufficient to penetrate through a protective coating and ensure contact with the conductive pad. However, repeated mechanical stress, poor needle alignment or mechanical degradation can damage the inner spring, inducing higher pressing forces on the test pads and consequently deeper indentations. This could

affect the integrity of the solder mask and/or expose underlying copper traces which potentially compromise the functionality and reliability of the board. Figure 1 illustrates an indentation created by a damaged needle, causing a much larger and deeper perforation on the test pad. The cross-section cut shows that the perforation exposed the copper traces eventually creating a short circuit.

The significant advancements in PCB inspection techniques using AOI, machine learning and deep learning algorithms have successfully identified PCB surface and solder joints defects. However, to the best of our knowledge there is no research concerning damage characterization caused by faulty needles during ICT tests. Besides, there are few open datasets of PCB defects available, and the few existing datasets mainly focus on component detection, cosmetic defect detection or solder joint defects. No dataset was found for characterization of needle damaged pads caused by ICT.

Therefore, the objective of this paper relies on the characterization of PCB damage caused by needle failure during the ICT test. Specifically, it aims to evaluate the viability of using computer vision and artificial intelligence to classify indentations as OK or NOK, allowing the identification of malfunction needles. By identifying NOK indentations, it would be possible to know which needles are responsible for producing them, while replacing the damaged needles avoids latent defects that could ultimately result in field failures.

B. Literature Review

Previous research in this field has mainly utilized computer vision (AOI), machine learning and deep learning for defect detection on PCBs. Automated Optical Inspection (AOI) systems utilize high-resolution cameras and image processing algorithms. It is one of the most widely used methods for detecting surface defects on PCBs, including open and short circuits [2], spurious copper, mouse bites[3] and other anomalies like solder joint defects, missing components, and misalignments [4]. However, AOI systems struggle with detecting internal defects and electrical connectivity issues, which still necessitate electrical testing methods. For non-visible defects in multi-layer PCBs, X-ray tomography and electromagnetic interference (EMI) analysis are commonly used. These techniques are particularly effective for identifying voids, microcracks, and hidden soldering defects in high-density interconnect (HDI) PCBs [5].

Many researchers have proposed several machine learning-based algorithms to improve traditional image processing methods. Most of them focused on solder joints or components defects detection and achieved good performances. The techniques applied include Support Vector Machines (SVM) [6], MLP neural network and geometric wavelet [7], AdaBoost and decision tree [8] and random forest pixel classifier [9].

Recent advancements in deep learning have significantly improved PCB defect detection. Unlike traditional machine vision methods, Convolutional Neural Network (CNN) approaches can automatically extract image features [10]. For surface defects detection, such as missing hole, mouse bite, open and short circuit, spur and spurious copper, researchers have successfully applied Faster R-CNN [11] and Feature Pyramid Networks (FPN) [12], as well as YOLO networks [13][14][15]. For solder joint defect detection, the most common methods include also CNNs [16] and YOLO [17].

Alternative testing approaches to ICT, such as contactless inspection methods, were also explored to minimize PCB damage. The authors of [1] have successfully utilized thermographic imaging in detecting microcracks and delamination by analyzing heat dissipation anomalies. Alternatively, [18] proposed using near electromagnetic (EM) field probing to identify missing components, shorts and overheating. On another approach, [19] present a non-contact infrared thermal signature analysis to detect defective components. While the proposed alternatives show promise in identifying component defects without requiring physical test points, further development is required to improve its measurement accuracy, automation and repeatability for high-volume PCB manufacturing. Despite the extensive

literature on AOI and learning-based inspection for PCB defects, ICT-induced pad indentations pose a different NDE problem: the damage can be subtle, highly dependent on probe condition and applied force, and may not manifest as a traditional “visual defect” until it becomes critical. In this context, inspection methods that are quantitative, repeatable, and traceable are required to support manufacturing decisions and prevent defect escapes. Optical microscopy is attractive because it is non-contact and can provide high-resolution evidence of surface integrity; however, to be manufacturing-relevant, it must be paired with a measurement methodology that yields calibrated features and actionable screening criteria rather than purely image-level predictions.

Therefore, this work proposes a metrology-driven optical NDE workflow for screening ICT-induced pad indentations. The approach combines a validated vision-based measurement pipeline with an interpretable classifier to distinguish acceptable from critical damage across different coatings, probe types, and force levels. By emphasizing quantitative features and measurement validation, the proposed method aims to bridge the gap between laboratory inspection and a deployable NDE screening step for electronics manufacturing.

The main contributions of this paper are:

- A quantitative, non-contact optical NDE workflow to detect and characterize ICT probe–induced indentations on PCB test pads.
- A validated vision-based metrology pipeline, benchmarked against reference measurements, achieving µm-level agreement and good repeatability.
- A curated dataset of > 2000 high-resolution images covering multiple pad coatings, probe types, and applied forces to study variability and robustness.
- An interpretable, feature-based screening model (decision tree) that achieves 98–100% accuracy for OK/NOK classification while remaining lightweight and traceable for industrial use.

II. METHODOLOGY

To address this problem, we propose an integrated instrumentation system for automated and vision-based characterization of indentation damage caused by ICT probe failure. This system combines robotic actuation, force calibration, high-resolution optical imaging and metrology-driven feature analysis. This section describes the methodology adopted to achieve the proposed objectives. It highlights the methods, workflow and equipments adopted throughout this research.

A. Experimental Setup

The proposed approach constitutes a complete measurement system for classifying and characterizing damage caused by ICT probe failures. The system integrates: robotic actuation with controlled force input, digital force sensing, optical metrology using a calibrated microscope and advanced feature extraction and classification based on AI algorithms.

There are several different types of probe needles commonly used on ICT tests that can vary in size, spring force, tip style, tip plating and tip diameter. For this study, two different needles were tested: ®PTR 1012EV2.8NH-AU-0.64-mS-B and 1025E-V-3.0NH-AU-0.9-mS, whose mechanical properties are indicated on TABLE I.

TABLE I Mechanical properties of the needles 1012 and 1025.

Properties	Series 1012	Series 1025
Full travel	6.40 mm	6.40 mm
Working travel	4.30 mm	4.30 mm
Spring force at working travel	2.8 N	3.0 N
Spring force at full travel	3.4 N	3.5 N

In total, five different types of PCBs were analyzed, each featuring distinct surface finishings, or coatings: Immersion Gold (ImAu), Immersion Tin (ImSn), and three variations of Organic Solderability Preservative (OSP) - ®Heraeus Type 3, ®Heraeus Type 4, and ®ALPHA Type 3. Each surface finish has its own purpose, which can be to enhance solderability (e.g., ImAu, ImSn), improve oxidation resistance (e.g., ImAu) or reduce manufacturing costs (e.g., OSP). Testing these variations has the purpose of understanding if there is any correlation between the coating of the PCB and the indentation created during ICT tests.

The PCB adopted in this study, regardless of the coating, is made up of six inner layers (copper foils have the thickness of 18 µm, 18 µm and 35 µm, 35 µm, 18 µm and 18 µm) with a theorical thickness of 1.55 mm. A collaborative robot UR10 was used as the actuator responsible for creating indentations on the PCBs. The robot's load cell was used to apply different forces on the test pad and an external digital force gauge (DFG) was mounted to measure and monitor the actual force applied on every test point of the PCB. As shown in Fig. 2, it was designed and 3D printed a jig to accommodate the needle on the DFG and another to couple the DFG on the robot. Images of the indentations were then captured using a DVM6 Leica Digital Microscope (optical resolution of about 1.67 micrometers per pixel). Although 3D scanners, such as LiDAR, or stereo cameras could be promising for the detection of such anomalies by providing indentation depth measurements, the needles release material residues upon ICT that make these measurements unreliable. The robot, load cell, microscope, and image analysis pipeline depicted in Fig. 3 constitutes a complete instrumentation and measurement system.

B. Workflow

The experimental trials were conducted according to the experimental setup previously explained. Each type of pad featuring different coatings was tested for both needle type and with different applied forces to simulate OK and NOK indentations. Although this threshold between OK and NOK indentations is still unknown, it was defined according to the needle's datasheet that indicates that the maximum force at full travel is 3.5 N (see TABLE I). For that purpose, the robot was programmed to apply 4 N and 5 N+, respectively. For programmed forces of 4N, the values read by the DFG were between 3 and 4 N (due to differences in the calibration of the robot's load cell). On the other hand, programming the robot for 5 N + resulted in random indentations from 5 to 12 N. In the end of the experiments, a full range of indentations between 3 and 12 N was achieved. The quantity of PCBs for each case scenario was defined according to the test pads existing in each different PCB in such a way that each coating-needle pair had around 200 images. This was the target number of samples defined to build a proper dataset, called ICT Probe-Induced Indentations on PCB Pads ($IPIP^2$) [20] that serve in the characterization process and achieving robust deep learning models

To generate the abovementioned dataset, the pipeline illustrated in Fig. 3 was implemented. *DL Model #1* is an AI-based segmentation model (YOLOv8) that distinguishes the pixels of interest (test point) from those belonging to the background (irrelevant areas). *DL Model #2* utilizes the YOLOv8 architecture optimized for segmentation tasks and serves to further refine the image by isolating the indentation from remaining information of the point test. *Processing Image Algorithm #1* fragments the test point into distinct zones (up to three) and quadrants (up to four). Zones are

numbered from 1 to 3, based on the distance from the center of pad, with zone 1 being the center. This step is necessary because the features of the indentations may vary depending on their location due to the test pad being slightly convex. *Processing Image Algorithm #2*, extracts a variety of features related to the indentation, including geometric attributes (the mean absolute error of the vision pipeline, when compared to reference measurements from the Leica DVM6, was 1.5 µm for height (2.1% MRE), with a bias of − 0.3 µm, indicating good agreement and low systematic deviation), shape, pixel intensity, and color-based properties. Moreover, the observed variation in indentation dimensions was below 2%, indicating good repeatability of the measurement method.

Both Processing Image Algorithms were developed using the Halcon computer vision library by MVTEC. These algorithms ensure high-performance image processing and feature extraction capabilities. This pipeline not only automates the characterization process but also accounts for the spatial distribution of the indentations, enabling a detailed and context-aware analysis of the dataset. The output of this pipeline is an Excel file containing over 500 columns, each representing a feature value. The number of rows corresponds to the number of images in the dataset. Additionally, the pipeline generates an edited image where the main features are visually highlighted for easy reference and consultation. Since the main goal of the project is to characterize OK and NOK indentations and many features may be redundant, decision trees were used to rank the most relevant ones based on their impact on classification.

Additionally, Principal Component Analysis (PCA) was applied to reduce dimensionality while retaining most of the variance. Though it does not indicate feature relevance for classification, it eliminates features from the dataset and facilitates further model's explicability. While PCA and decision tree serve different purposes, decision threes also point out the most relevant features and offer an easy way of interpreting how the AI classification model internally operates. To compare both dimensional reduction approaches, two decision trees were built for each coating-needle pair: the first using all the features and the second using only those selected by the PCA.

As indentations have complex patterns, a more powerful deep learning-based model was introduced to evaluate which approach, as classifier, is the most suitable for distinguishing OK and NOK test points. The Deep Learning model selected was YOLOV8 from the YOLO family, a widely known model that offers satisfactory trade-offs between accuracy and inference time, which makes it suitable for applications requiring real-time processing. Therefore, the performance of those decision trees and the deep learning classification models are further compared.

TABLE II Total samples by coating-needle pair.

PCB Coating	Series 1012	Series 1025
OSP Heraeus Type 3	192	264
OSP Heraeus Type 4	183	278
OSP Alpha Type 4	258	303
ImAu	190	190
ImSn	219	214
TOTAL	1042	1249

IV. EXPERIMENTAL RESULTS AND ANALYSIS

This chapter describes the dataset generated and the sub consequent configurations analysis.

A. Dataset description

TABLE **II** shows the number of samples for each coating- needle pair present in the dataset created for this study. IPIP^2 dataset [20] has the goal of having around 200 samples per coating-needle pair was assured. In the last table differences can be observed differences between the number of samples across different coatings. It is due to the fact that the PCBs had a different number of test pads. Nevertheless, for each coating-needle combination, a balanced dataset was obtained, consisting of approximately 50% of indentations up to 4 N and 50% ranging from 5 to 12 N. This dataset is published in

B. OSPHT3 – Needle 1025 (OK indentations ≤ 4 N & NOK Indentations > 4 N)

For this first analysis were only considered indentations for the coating-needle pair OSPHT3-1025 and the threshold between OK and OK was set at 4N. The dimensionality reduction technique PCA was applied and a decision tree model was trained both with and without incorporating the PCA results. In the later decision structure, the dataset is not filtered by PCA, meaning the classifier model was trained using all 512 features. From this training process, the model identified a very small subset of features considered relevant. The same process was repeated for a subset of features identified by PCA as relevant for the context, totaling 55 features. The resulting decision tree is more complex and utilizes a greater number of features compared to the previous model. This knowledge base is divided into three subsets: training, evaluation, and testing, comprising 70%, 15%, and 15% of the total data, respectively. The performance metrics show that the classification model trained with the subset of features suggested by the prior applied PCA leads to lower performance than the model that processes all features in the dataset (98.48% vs 100% accuracy). In the latter approach the decision tree determines internally which features are relevant. While the PCA technique points out features related to pixel intensity patterns or indentation geometry shape, the decision three that process all features highlights some metrology-based features. The results showed that the decision tree, to offer maximum accuracy, applies more weight to the feature *height*. It is important to note that the training process utilizes all indentation samples without segregating them by region. However, as will be demonstrated, indentation features may vary across different zones. Therefore, follows an analysis of certain relevant features for each of the three possible zones where the indentations predominantly occur.

i. Features analysis – zone 1

Figure 4 presents the density plots illustrating the feature value distribution of the dataset and estimated probability density function for the three different possible zones. The plot also highlights where the data for OK and NOK indentation samples are concentrated. This visualization demonstrates why this

height feature of the indentation dataset is the most critical for classification in the AI model: the overlap between the density plots is relatively small, and the peak values (modes) are distinct and significantly separated. At the zone 1, for example, there is a clear peak value difference, that corresponds to 0.05923 mm.

Figure 5 and Fig. 6 present density plots for additional features. While some of these features may not rank among the most relevant, they are easily interpretable and commonly used in similar problems, particularly in scenarios where AI models are not applied and a human-driven feature engineering approach is followed. The results indicate that the features width and maximum diameter could play a significant role in the classification process, unlike perimeter which shows a high probability of overlapping in values between the two indentation classes. As expected, NOK indentations exhibit a more regular geometric shape, resembling a polygon, leading to moderate values for rectangularity and circularity features. Regarding the convexity feature, both indentations classes present high values. NOK indentations have a shape closer to a rectangle, which might be related to its aspect ratio.

ii. Features analysis – zones 2 and 3

The graphs of Fig. 4 indicate that this feature is also relevant for the classification of indentations located outside zone 1, as the overlap of both OK and NOK densities is low for zones 2 and 3. This suggests that regarding the zone, OK and NOK indentations have distinct distributions, making it unlikely for them to share the same feature values. However, results suggest that indentations located close to the center of the test point are more likely to be accurately classified, as the peak frequency of height values shift closer when indentations occur further from the center. Regarding the dimensional features perimeter, width and maximum diameter, the conclusions are aligned with the analysis from zone 1. Both width and maximum diameter have the potential to help classification models in distinguishing indentations classes, whereas perimeter does not contribute significantly to this differentiation. The width values distribution revealed that the mode value difference between OK and NOK indentations remains practically unchanged across different zones. However, the maximum diameter peak difference increases in regions farther from the center of the test point. In contrast, the distribution for zone 1 lacks a clear peak, as this feature exhibits a wider range of possible values. The perimeter feature analysis indicates that the overlap area between indentations class values has increased. The density graphs for remaining features plots present similar patterns to those described in zone 1, as the level of overlap between density graphs are similar with very small changes in the range of possible values, while the peak values practically remained unchanged. The previous analysis indicates that the geometry shape features of the indentations practically do not change across different zones, unlike the physical dimension. The peak value decreases for indentation located furthest of the center of the test point suggesting that distinguishing indentations closer to the center is easier than those in other locations.

iii. Artificial intelligence algorithm performance analysis

As previously discussed, decision trees relying on metrology-based features achieve optimal classification performance. Nevertheless, it was also tested a deep learning-based model for the classification task, YOLOV8, which was trained with segmented indentations properly labelled. Two versions of the same YOLO architecture, the nano and medium, were trained using various combinations of hyperparameters. However, there are many other approaches to improve the performance of deep learning models, including testing more combinations of hyperparameters values.

TABLE III shows the performance metrics for YOLOv8. Even though deep learning models are more complex (which generally gives them the ability to encode more complex patterns), the results in TABLE III indicate that both YOLOv8 and decision tree that relies in the PCA analyses have poorer results than the simple decision tree. This indicates that distinguishing OK from NOK indentations for the coating needle pair doesn't require complex AI architectures. Simple architectures such as machine learning models are suitable as long as the most relevant features are properly identified.

TABLE III

Classification models performance metrics for coating-needle pair OSPHT3-1025.

Classification Model	**YOLOv8 Nano**	**YOLOv8 Large**	**Decision Tree**	**DT with PCA**
Accuracy (%)	84.62	88.46	100	98.48

A. OSPHT3 – Needle 1025 with different thresholds for OK and NOK forces

As stated before, the true threshold between OK and NOK indentations is unknown. Thus, the objective is to effectively distinguish indentations caused by different applied forces. According to the problem analysis and past discussions, the needle force at the ICT inspection does not gradually increase in order to allow the application of proactive

malfunction detection system. For this reason, various thresholds of OK and NOK forces were tested. Keeping the OK indentations as 4 N or less, studies A, B and C classified NOK indentations those exceeding 5, 6 and 7 N respectively. For the purpose of this analysis, intermediate values were ignored (i.e., 4–5, 4–6 and 4–7 N for studies A, B and C, respectively).

TABLE IV presents the difference between the high frequency values for different thresholds of forces of the height feature - identified as the most significant feature for distinguishing the two classes of indentations – and also for width and maximum

diameter, equally considered as relevant features. The results of TABLE IV reveal that the difference between peak values of the height feature increases as the gap between OK indentations and NOK indentations becomes larger, suggesting that the higher the gap the higher the classification model's performance is expected to be. However, the performance metrics suggested the opposite. For instance, the accuracy metric reported values of 100%, 98.09% and 97.90% respectively for Study A, B and C. This can be explained by the fact that as the gap between OK and NOK indentations increases, there's a reducing number of samples for NOK indentations on the dataset, leading to a problem called dataset imbalance. Therefore, this result does not imply that the decision tree is not suitable for a scenario where NOK indentations result from forces exceeding 7 N. It might indicate instead that more samples are required to properly train the model and, consequently, test its performance. Alternatively, reducing the number of OK samples can be tested as a dataset balance strategy.

TABLE IV

Value peak differences between OK and NOK samples, given in mm, for different thresholds force values.

Features	**Study A: OK (≤ 4 N) & NOK (≥ 5 N)**	**Study B: OK (≤ 4 N) & NOK (≥ 6 N)**	**Study C: OK (≤ 4 N) & NOK (≥ 7 N)**
Height Peak Difference	0.06087	0.06249	0.06315
Width Peak Difference	0.02280	0.02942	0.03089
Diameter Peak Diff.	0.05930	0.05998	0.06034

A. *Other coating-needle pairs*

The approach used for the previous coating-needle pair is the same as followed in this subsection, but in this case only the results are presented. As anticipated, there are instances where the most relevant feature is not metrology-based. However, the extracted variables values demonstrate that, in the case of ImAu and ImSn materials, the density graphs for height and width tend to be further apart, reducing the probability of overlapping values. This phenomenon does not seem to occur for the remaining materials, and it might result from the fact of the ImAu and ImSn test point being fully flat, unlike the remaining where the pad surface is convex. Moreover, the indentations on material ImAu and ImSn tend to be smaller in dimensions than on the other materials.

TABLE V summarizes the maximum achieved performance in terms of accuracy of the developed decision tree (DT), decision tree with PCA and also the deep learning model (DL). The conclusions from TABLE V are also valid for the remaining coating-needle pairs: decision tree can achieve satisfactory performance on the task of classifying OK and NOK

TABLE V

Performance metrics (accuracy) achieved by a.i. models for two different needles and conditions.

	OK (≤ 4 N) & NOK (> 4 N)						OK (≤ 4 N) & NOK (≥ 5 N)					
	Needle 1012			Needle 1025			Needle 1012			Needle 1025		
	DT	PCA	DL	DT	PCA	DL	DT	PCA	DL	DT	PCA	DL
OSP Heraeus Type 3	100	100	89.47	100	98.48	88.46	97.88	95.77	94.74	100	98.33	91.67
OSP Heraeus Type 4	100	100	94.44	98.56	100	82.14	100	100	94.44	100	96.55	95.65
OSP Alpha Type 4	100	100	96.15	100	100	90	97.37	96.05	92	100	98.47	92.31
ImAu	100	100	94.74	100	100	88.89	100	100	100	100	100	100
ImSn	100	100	100	100	100	100	100	100	95.45	100	100	100

indentations. However, in these cases, the maximum gap between OK and NOK forces is smaller than in the previous analysis. The decision tree with PCA has more complexity than the one that processes all the features and surprisingly achieved. worst performance. It indicates that the decision tree was more efficient in the selection of the most relevant features. When comparing with the deep learning model, the results reaffirm that the simplest and least complex classification model consistently delivers the best performance, regardless of the coating-needle pair or scenario (threshold forces separating OK from NOK indentations).

V. CONCLUSION

This study evaluated the impact of ICT test probe failures on the indentations left on PCB test pads. Over 2,000 images were collected through experimental trials combining different PCB surface finishes (OSP, ImAu, ImSn), probe types, and applied forces, enabling a comprehensive analysis of their individual effects.

Results confirmed the feasibility of using computer vision and AI to classify indentations as OK or NOK. Simple decision tree models using all available features outperformed PCA-based approaches and even advanced models like YOLOv8. Among features, indentation height proved to be the most significant for accurate classification. It was also observed that indentations located farther from the pad center tend to exhibit lower feature overlap, simplifying classification.

The experimental setup, however, lacked the precision to control indentation position. Empirical data and needle datasheets revealed that probe failures occur abruptly, without prior warning, often resulting in forces exceeding 7N and causing deep damage. As the gap between OK and NOK forces increases, the difference in peak height values also grows, improving model performance.

The findings demonstrate that vision-based inspection and metrology solutions can effectively mitigate PCB damage due to ICT probe failures. Although the measurement system used was suited only for laboratory conditions, the variables analyzed serve as valuable guidelines for specifying industrial-grade vision setups. Based on the measured separation between OK and NOK damage, commercially available vision cameras can meet the required specifications.

This research advances both the theory and practical application of automated measurement and inspection in industrial settings, showing that interpretable and traceable vision systems can help reduce failures in production lines.

Declarations

Author Contribution

R.S., A.S., L.C. and C.L. conduct the research and development tasks and wrote the main manuscript text, A.A P.P and D.F reviewed the manuscript and coordinated the research, A.A. provided physical resources such as PCBs and laboratory facilities and validated the dataset and developments outputs

Acknowledgement

This work was supported under the base funding project of the DTx CoLAB, under the Missão Interface of the Recovery and Resilience Plan (PRR), integrated in the notice 01/C05-i02/2022, which aims to deepen and consolidate the network of interface institutions between the academic, scientific and technological system and the Portuguese business fabric.

Data Availability

article data were deposited into the Mendeley data database under DOI number 10.17632/kx2sc9ht3c.2 and are available at the following URL: https://data.mendeley.com/datasets/kx2sc9ht3c/3

Competing interest

The authors declare no competing interests

References

1. Jeon, M., Yoo, S., Kim, S.W.: A Contactless PCBA Defect Detection Method: Convolutional Neural Networks with Thermographic Images, *IEEE Trans Compon Packaging Manuf Technol*, vol. 12, no. 3, pp. 489–501, Mar. (2022). 10.1109/TCPMT.2022.3147319
2. Pal, A., Chauhan, S., Bhardwaj, S.: Detection of Bare PCB Defects by Image Subtraction Method using Machine Vision, *Proceedings of the World Congress on Engineering 2011, WCE 2011*, vol. 2, Jul. (2011)
3. Ma, J.: Defect detection and recognition of bare PCB based on computer vision, in *36th Chinese Control Conference (CCC)*, 2017, pp. 11023–11028. (2017). 10.23919/ChiCC.2017.8029117
4. Ulger, F., Yuksel, S.E., Yilmaz, A., Gokcen, D.: Solder Joint Inspection on Printed Circuit Boards: A Survey and a Dataset. IEEE Trans. Instrum. Meas. **72** (2023). 10.1109/TIM.2023.3277935
5. Tan, C.M., Chen, H.H., Wu, J.P., Sangwan, V., Tsai, K.Y., Huang, W.C.: Root Cause Analysis of a Printed Circuit Board (PCB) Failure in a Public Transport Communication System. Appl. Sci. (Switzerland). **12**(2) (Jan. 2022). 10.3390/app12020640
6. Yun, T.S., Sim, K.J., Kim, H.J.: Support vector machine-based inspection of solder joints using circular illumination. Electron. Lett. **36**(11), 949–951 (May 2000). 10.1049/el:20000342
7. Acciani, G., Brunetti, G., Fornarelli, G.: Application of neural networks in optical inspection and classification of solder joints in surface mount technology. IEEE Trans. Industr Inf. **2**(3), 200–209 (2006). 10.1109/TII.2006.877265
8. Hongwei, X., Xianmin, Z., Yongcong, K., Gaofei, O.: Solder Joint Inspection Method for Chip Component Using Improved AdaBoost and Decision Tree. IEEE Trans. Compon. Packaging Manuf. Technol. **1**(12), 2018–2027 (2011). 10.1109/TCPMT.2011.2168531

9. Li, D., Li, C., Chen, C., Zhao, Z.: Semantic Segmentation of a Printed Circuit Board for Component Recognition Based on Depth Images. Sensors. **20**(18) (2020). 10.3390/s20185318
10. Ling, Q., Isa, N.A.M.: Printed Circuit Board Defect Detection Methods Based on Image Processing, Machine Learning and Deep Learning: A Survey. IEEE Access. **11**, 15921–15944 (2023). 10.1109/ACCESS.2023.3245093
11. Ding, R., Dai, L., Li, G., Liu, H.: TDD-Net: A Tiny Defect Detection Network for Printed Circuit Boards. CAAI Trans. Intell. Technol. **4** (May 2019). 10.1049/trit.2019.0019
12. Hu, B., Wang, J.: Detection of PCB Surface Defects With Improved Faster-RCNN and Feature Pyramid Network. IEEE Access. **8**, 108335–108345 (2020). 10.1109/ACCESS.2020.3001349
13. Adibhatla, V.A., Chih, H.-C., Hsu, C.-C., Cheng, J., Abbod, M.F., Shieh, J.-S.: Defect Detection in Printed Circuit Boards Using You-Only-Look-Once Convolutional Neural Networks. Electron. (Basel). **9**(9) (2020). 10.3390/electronics9091547
14. Liao, X., Lv, S., Li, D., Luo, Y., Zhu, Z., Jiang, C.: YOLOv4-MN3 for PCB Surface Defect Detection. Appl. Sci. **11**(24) (2021). 10.3390/app112411701
15. Zhou, W., et al.: An Efficient Tiny Defect Detection Method for PCB with Improved YOLO Through a Compression Training Strategy. IEEE Trans. Instrum. Meas. **73**, 1–14 (2024). 10.1109/TIM.2024.3390198
16. Sezer, A., Altan, A.: Detection of solder paste defects with an optimization-based deep learning model using image processing techniques, *Soldering and Surface Mount Technology*, vol. 33, no. 5, pp. 291–298, Oct. (2021). 10.1108/SSMT-04-2021-0013
17. Li, Y.-T., Kuo, P., Guo, J.-I.: Automatic Industry PCB Board DIP Process Defect Detection System Based on Deep Ensemble Self-Adaption Method. IEEE Trans. Compon. Packaging Manuf. Technol. **11**(2), 312–323 (2021). 10.1109/TCPMT.2020.3047089
18. Alaoui, N.E.B., Tounsi, P., Boyer, A., Viard, A.: New testing approach using near electromagnetic field probing intending to upgrade in-circuit testing of high density PCBAs, in *IEEE 27th North Atlantic Test Workshop (NATW)*, 2018, pp. 1–8. (2018). 10.1109/NATW.2018.8388867
19. Alaoui, N.E.B., Tounsi, P., Boyer, A., Viard, A.: Detecting PCB Assembly Defects Using Infrared Thermal Signatures, in *MIXDES – 26th International Conference Mixed Design of Integrated Circuits and Systems*, 2019, pp. 345–349. (2019). 10.23919/MIXDES.2019.8787089
20. Silva, R., et al.: ICT Probe-Induced Indentations on PCB Pads - IPIP2. Mendeley Data. (2026). 10.17632/kx2sc9ht3c.3

Figures

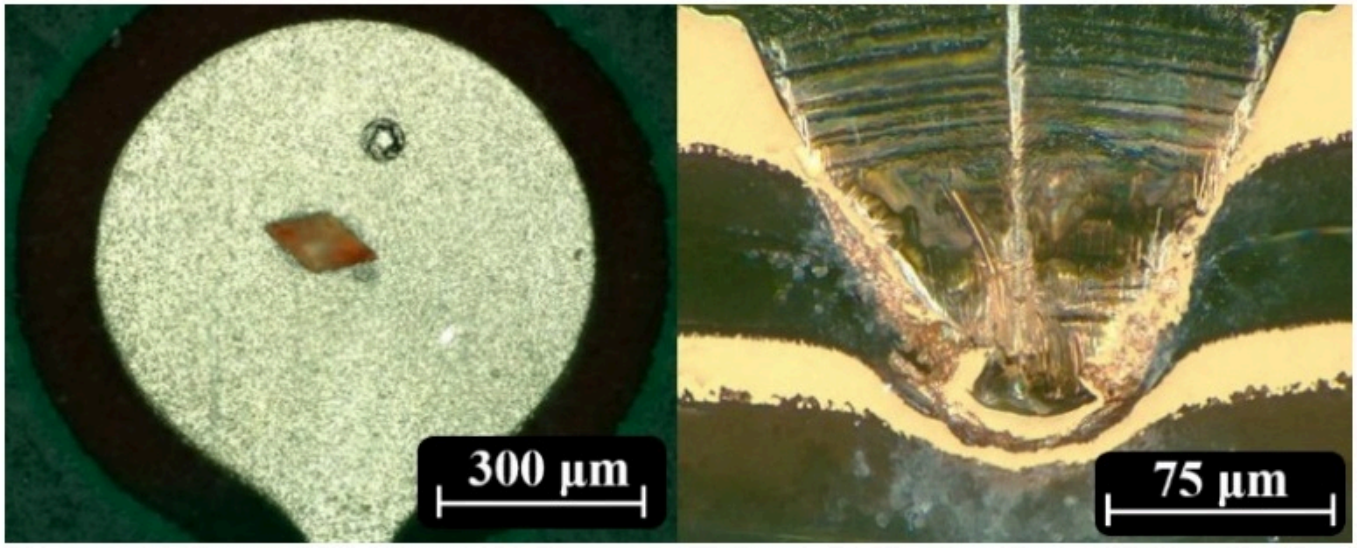


Figure 1

Example of a critical indentation on a test pad caused by a faulty needle on ICT test (left); and a metallographic cross-section revealing exposed copper traces and consequent short circuit (right).



Figure 2

Experimental setup used to create indentations on the PCBs.

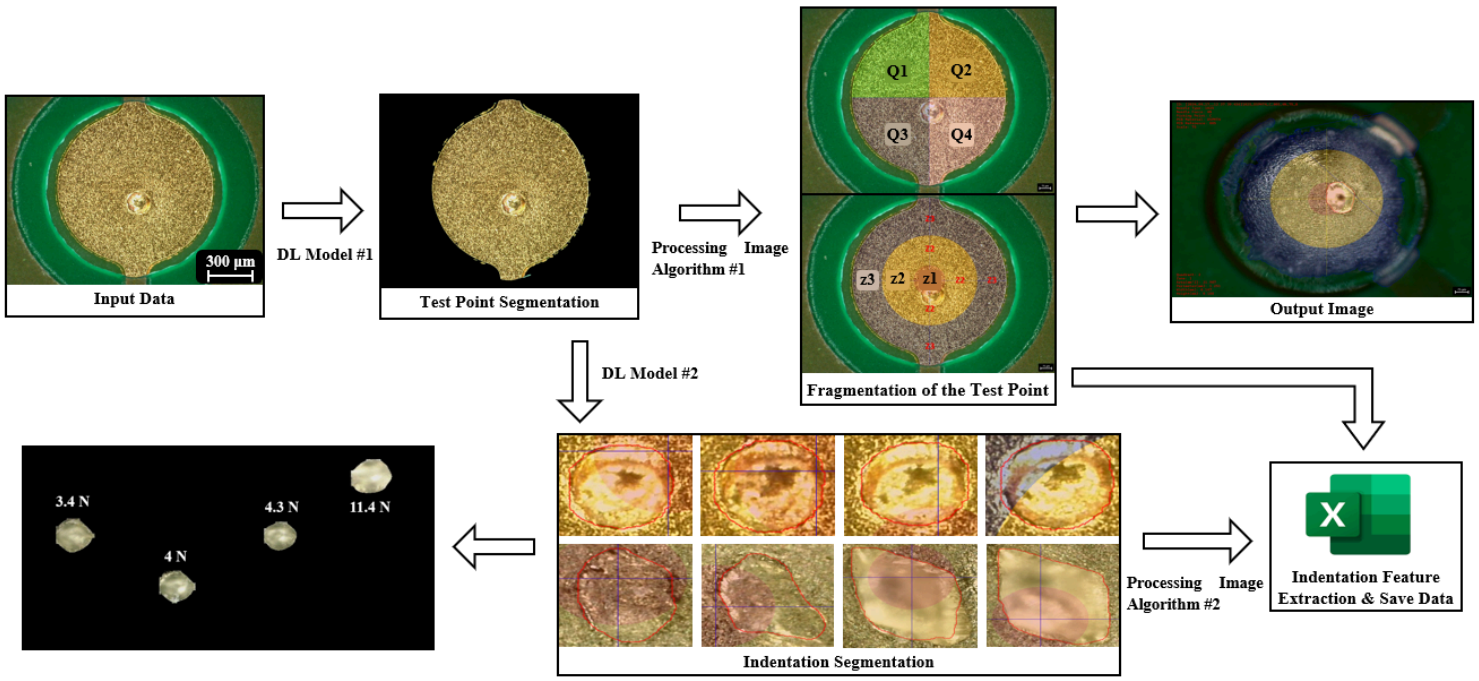


Figure 3

Overview of the image processing and feature extraction pipeline for automatic generation of a dataset linking features to OK and NOK labels

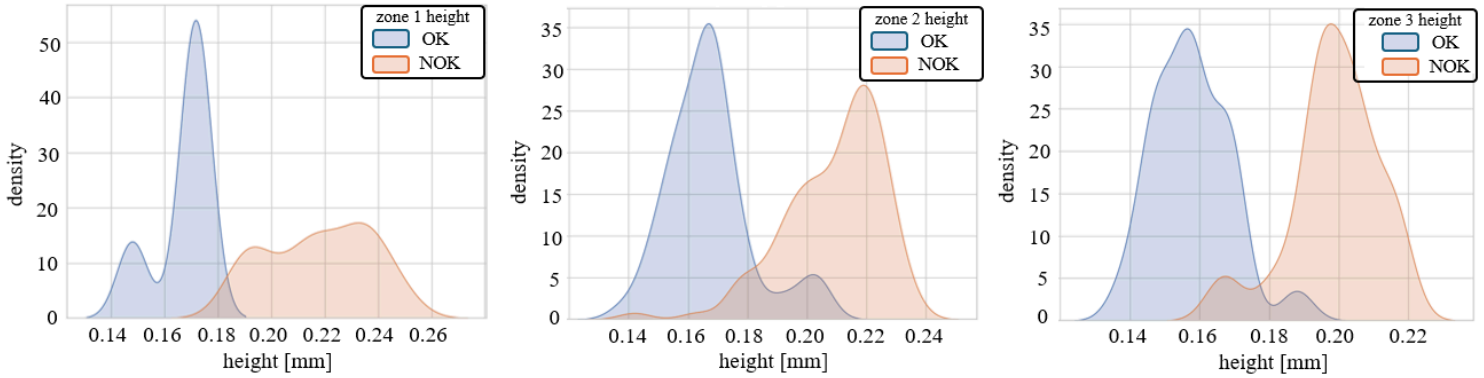


Figure 4

Density plots for height feature (given in millimeters) for OK and NOK indentations samples for coating-needle pair OSPHT3-1025 located at zone 1, 2 and 3 respectively at left, center and right.

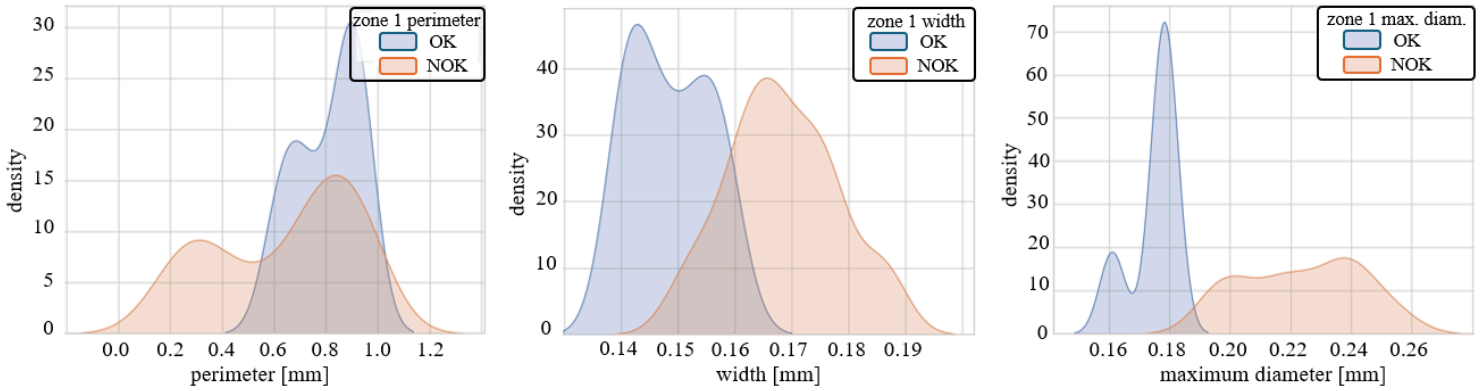


Figure 5

Density plot for perimeter, width and maximum diameter feature values (respectively, from left to right), given in millimeters, measured for samples of OK and NOK indentations located at zone 1 for OSPHT3-1025 pair samples.

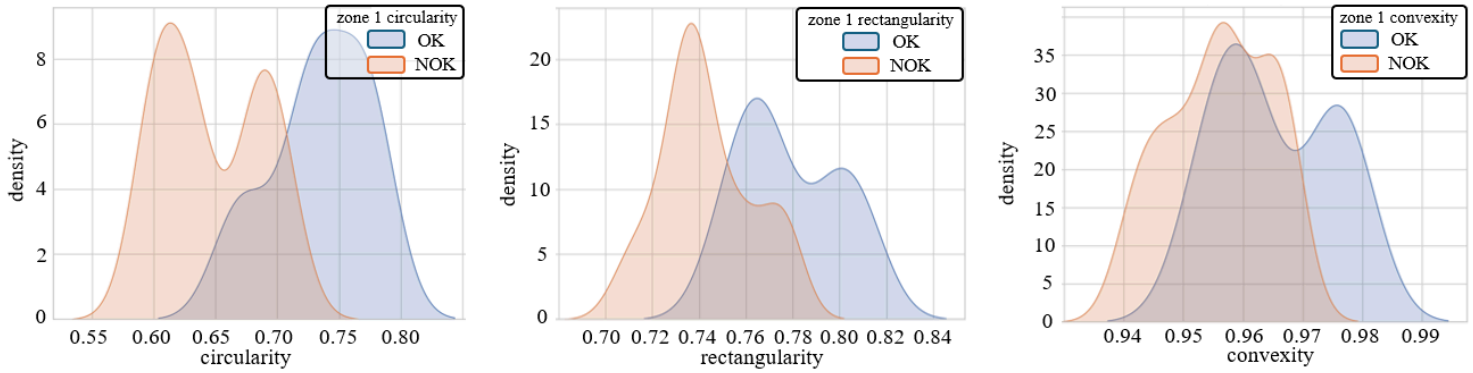


Figure 6

Density plot for circularity, rectangularity and convexity feature values (respectively from left to right) of OK and NOK samples found at zone 1 for OSPHT3-1025 pair samples.